Using 3D numerical simulations to model active in-mine seismic surveys at South Deep Gold Mine, South Africa

by S. Plaatjie, M.S.D. Manzi, L. Linzer, M. Sihoyiya

Affiliation:
University of the Witwatersrand, Johannesburg, South Africa

Correspondence to:
S. Plaatjie

Email:
810385@students.wits.ac.za

Dates:
Received: 20 Jun. 2024
Revised: 31 Dec. 2024
Accepted: 22 Jan. 2025
Published: January 2025

How to cite:
Plaatjie, S., Manzi, M.S.D., Linzer, L., Sihoyiya, M. 2025. Using 3D numerical simulations to model active in-mine seismic surveys at South Deep Gold Mine, South Africa. *Journal of the Southern African Institute of Mining and Metallurgy*, vol. 125, no. 1, pp. 43–50

DOI ID:
http://dx.doi.org/10.17159/2411-9717/3473/2025

ORCiD:
S. Plaatjie
http://orcid.org/0000-0002-7161-8129
M.S.D.Manzi
http://orcid.org/0000-0002-1654-5211
L. Linzer
http://orcid.org/0000-0003-1581-0420
M. Sihoyiya
http://orcid.org/0000-0003-1956-5223

Abstract

Fiber-Optic Sensing and UAV-Platform Techniques for Innovative Mineral Exploration (FUTURE) is a joint European Union and South African consortium project funded under ERA-NET Cofund ERA-MIN3. The project aims to develop cost-effective and novel seismic methods to image geological structures ahead of the mine face, ultimately leading to improved decision-making and safer mining practices. In this study we present results from numerical simulations conducted at South Deep Gold Mine for active in-mine seismic surveys. The study uses a finite differencing code known as WAVE3D, which models models the propagation of a seismic wave generated by stress pertubations that are applied to a defined grid. The numerical simulation model included two major ore bodies (Black Reef and Ventersdorp Contact Reef) and mine tunnels. The model was constrained using laboratory physical property measurements from underground borehole samples such as seismic velocities (e.g., compressional and shear waves) and bulk densities. Two case studies were created, one modelled the active shots and receivers on surface, and the other modelled the shots at depth (in a mine tunnel at ~4000 m depth) with receivers on surface. In both cases, the objective was to investigate the wavefield propagation through the rockmass between the mine tunnel and surface. The simulated wavefield produced by the source located along the mine tunnel was successfully recorded on surface. The surface-recorded wavefield exhibits clear one-way P-wave arrival times at approximately 450 ms to 500 ms, which can be used to calculate the surface-tunnel P-wave refraction tomogram. The numerical simulation results from the study were used to optimise the acquisition parameters of the in-mine seismic surveys conducted under the FUTURE project.

Keywords

mining, mine design, layouts, numerical simulation, seismic surveys

Introduction

South Africa hosts some of the world's deepest gold mines, with some mines operating at depths close to 4000 m below ground surface. Due to these great depths and high stresses, mine personnel are exposed to risks such as rockbursts, falls of ground and other hazardous conditions linked to the presence of geological structures (e.g., faults and dykes). Furthermore, mining-related accidents affect mining operations and slow productivity. Hence, understanding rock mass behaviour at these depths is a priority for the gold mining industry.

One of the techniques used to map the subsurface gold-bearing horizons in the Witwatersrand Basin is the seismic reflection method (e.g., Durrheim et al., 1991; Gibson et al., 2000; Manzi et al., 2013). However, conducting seismic surveys can be very costly and time consuming and may, in the case of brownfield exploration projects, interfere with the mining operations. Consequently, it has become increasingly useful to optimise the design of seismic surveys by prior numerical simulation. The simulations may be used to study and predict the behaviour of the seismic waves as they propagate through the rock mass. In particular, this computational approach aids the planning of in-mine seismic surveys where there are limited opportunites to place source and sensors. In this study we show how numerical simulations can be used to plan and aid the design of surface and tunnel reflection seismic surveys based on the site geology, infrastructure (i.e., mine tunnel) and laboratory physical property measurements.

This study is part of the Fiber-Optic Sensing and UAV-Platform Techniques for Innovative Mineral Exploration (FUTURE) project, which is an international consortium project funded by the European Union (EU) and South Africa (SA), aimed at developing cost-effective and novel seismic methods for deep mineral exploration, mine planning and development.

Using 3D numerical simulations to model active in-mine seismic surveys at South Deep Gold Mine

One of the challenges of conducting in-mine seismic surveys are mining activities that may limit access to regions of interest and also introduce noise to the data. This noise can be introduced by moving vehicles, machinery, blasting, and other mining-related operations. The simulation of seismic surveys can avoid these challenges since we only work with the elements we compute in our model. Not only does this approach ensure that we simulate the processes that we are interested in, but it is cost-effective and efficient. Thus, using these 'idealistic' mine conditions, we are able to extract useful information from numerical simulations to constrain the design, acquisition and processing of the in-mine seismic data.

The study aims to answer the following key questions:

- Is it possible to detect on surface the seismic wave field originating from deep underground mine tunnel (~4000 m) to characterise gold-bearing horizons, geological structures (faults, sills, and dykes) and rockmass between surface and tunnel floor?
- How do the downward and upward going seismic wavefields interact with the subsurface lithologies, mine infrastructure, and complex geological structures with significantly different physical properties?
- Is it possible to conduct time sychronised surface-tunnel seismic surveys for mineral exploration, mine planning, and development?

Geological background

The study area is located 45 km southwest of Johannesburg in South Deep Gold Mine, which is situated on the northwestern rim of the Witwatersrand Basin (Figure 1). The mine is an intermediate to ultradeep level operation with two shaft systems (Figure 2). It operates between 2000 m and 4000 m below the surface, exploiting the Ventersdorp Contact Reef (VCR) and Upper Elsburg Reefs.

Karoo Supergroup sandstones and shales crop out in the mining right area. The Transvaal Supergroup, comprising the Pretoria and Chuniespoort groups, underlie the Karoo Supergroup rocks. The Chuniespoort Group consists of dolostones, quartzites, and shales (Gibson et al., 2000; McCarthy, 2006). The basal layer of the Tranvaal Supergroup is the relatively thin Black Reef Formation (BLR) (ca. 2588±6 Ma, Krapež, 1985; Vos, 1975; Jolly et al., 2004).

The Ventersdorp Supergroup (ca. 2.72–2.63 Ga) lies beneath the BLR. It includes the amygdaloidal basaltic lava's Pniel sequence (Van der Westhuizen et al., 1991), metasedimentary rocks and bimodal volcanics of the Platberg Group, as well as ultramafic and mafic rocks from the Klipriviersberg Group (Van der Westhuizen et al., 199 1; Manzi et al., 2012). The Ventersdorp Contact Reef (VCR) (ca. 2729±19 Ma, Kositcin and Krapez, 2004; U–Pb detrital zircon SHRIMP) is one of the orebodies mined at South Deep Gold Mine and represents a significant geological marker in the Witwatersrand Basin. It is part of the Ventersdorp Supergroup and comprises a thin fluvial auriferous conglomerate (Gibson, 2004, 2005; McCarthy, 2006).

The VCR is underlain by the Witwatersrand Supergroup, which comprises coarse clastic rocks and bimodal volcanic rocks. The Witwatersrand Supergroup is divided into two main groups: the Central Rand Group and the West Rand Group. The Central Rand Group (ca. 2902 – 2849 Ma, Kositcin and Krapez, 2004; U–Pb detrital zircon SHR-IMP), consists of sandstone, conglomerate, and shale units and unconformably overlies the West Rand Group. The Central Rand Group is divided into two subgroups, namely the upper Johannesburg Subgroup and the lower Turffontein Subgroup. It is significant because it hosts the majority of the auriferous reefs mined in South Deep Gold Mine and across the basin (De Kock, 1964; Manzi et al., 2013).

The West Rand Group (ca. 2984 – 2902 Ma; Kositcin and Krapez, 2004, U–Pb detrital zircon SHRIMP), which is composed

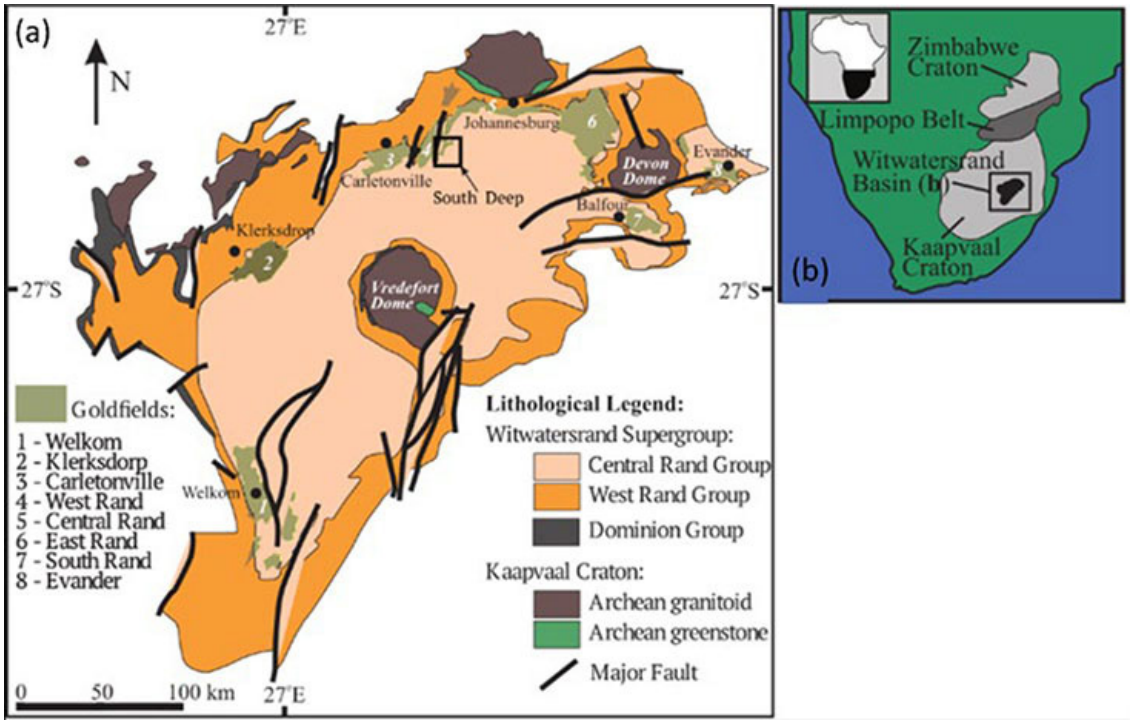

Figure 1—A geological map of the Witwatersrand Basin showing the location of the (a) South Deep Gold Mine and (b) the map of Southern Africa showing the Cratons (Nwaila, 2021)

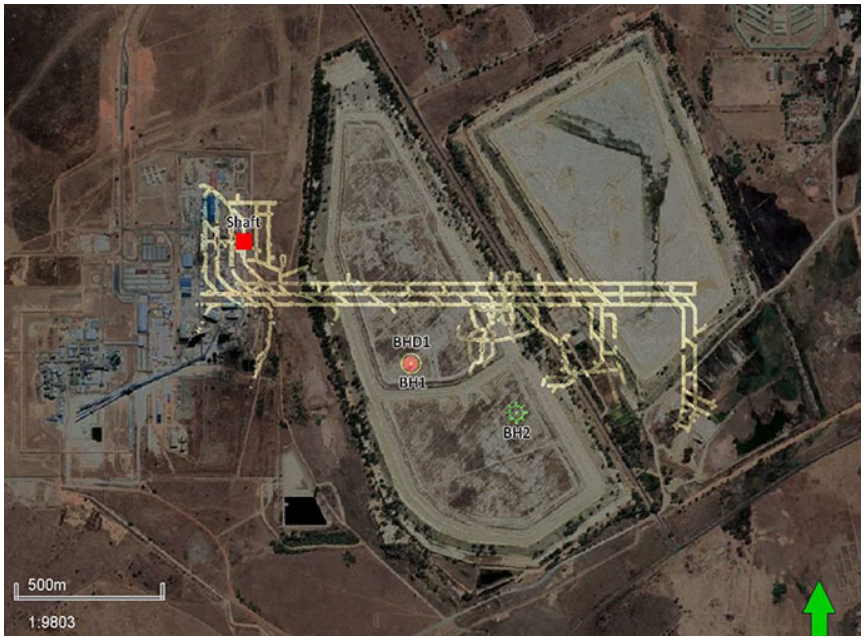

Figure 2—A satellite map showing the South Deep Gold Mine, the shaft used to access the mining levels and the location of the boreholes BH1, BHD1 (deviation of BH1), and BH2, which produced the 24 samples taken from our study area

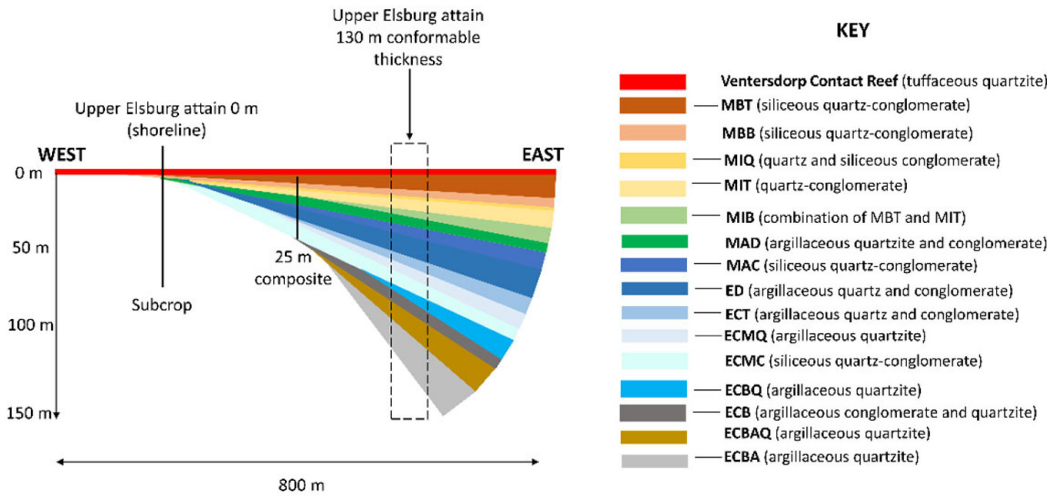

Figure 3—Illustration of the clastic wedge model from the Upper Elsburg model of the South Deep Gold Mine

of clastic and predominantly marine metasedimentary rocks, unconformably overlies the Dominion Group (ca. 3074 ± 6 Ma), (Myers et al., 1989). The West Rand Group is further subdivided into three formations: the Jeppestown, Government and Hospital Hill Subgroups (Manzi et al., 2013). The region is also dominated by multiple fault systems such as the north-south trending Panvlakte, West Rand and Wrench Fault systems.

The base of the Ventersdorp Supergroup, the Ventersdorp Contact Reef (VCR), is a strong seismic marker across the basin and it is used as a proxy seismic reflection to constrain the depth and location of the seismically transparent Upper Elsburg Reef (UER) at South Deep Gold Mine (Manzi et al., 2013). The Upper Elsburg reefs are made up of the Upper Elsburg Individuals (Waterpan Member) and the Upper Elsburg Massives (Modderfontein Member). The borehole data reveal that the members attain a maximum combined thickness of 130 m towards the east of the site (see Figure 3).

Methodology and results

Physical properties

In order to understand how seismic waves propagate in the study area, an analysis of the laboratory ultrasonic velocities and bulk densities of our samples was conducted. Other physical property measurements used in the study were obtained from the previous studies (e.g., Manzi et al. 2013). The information obtained from the analysis was used in conjuction with mine geometry and geological information to conduct numerical simulations. The 24 samples were collected from three lithologically diverse boreholes spanning the study area (Figure 2). All the boreholes (BH1, BHD1, and BH2) are drilled from the underground workings and intersect the reefs of interest. The borehole BH1 intersects the Modderfontein members (MBT, MBB, MIT, MIQ, MIT, MAD, MAC) and the overlying VCR for 26.6 m and intersects the Waterpan Members (ED, ECT, ECMQ, ECBQ, ECB, ECBAQ, ECBA) for 227.5 m. The borehole BHD1

intersects the Modderfontein Members, including the overlying VCR, for 77.69 m and intersects the Waterpan Members for 291.96 m. The most easterly borehole, BH2, intersects the Modderfontein Member including the VCR for 33.67 m and Waterpan Member for 156.33 m.

Elastodynamic modelling

We used a three dimensional finite differencing code known as WAVE3D (Hildyard et al., 1995) which models the propagation of a seismic wave generated by a stress pertubation that is applied to a defined grid. The code does this by solving the elastodynamic wave equation and then calculating the displacements, velocities and stresses at all points in the staggered grid that are induced by the wave field as it propagates. The mesh equations are solved with fourth order accuracy in space, although this reduces to second order at boundaries and discontinuities. The fourth order system provides comparable accuracy to the second order method with a finer mesh (Linzer et al., 2021).

Source models in WAVE3D

Active sources are predefined stress distributions in space and time (dilatational or shear) that are enforced either internally at mesh points or on discontinuity surfaces (Linzer et al., 2021). Choosing an appropriate representation of the source, which introduces frequencies of disturbance into the mesh, has implications for the size and number of grid components. The finite difference scheme suffers from the dispersion of higher frequencies. When defining the source, three factors must be considered: its shape, pulse duration, and region of coverage. These are chosen so that the frequencies in the mesh meet a criterion, ensuring that frequencies below this criterion don't exhibit considerable dispersion within the propagation distances under consideration. The grid element size and source frequency are coupled parameters, meaning the choice of one constrains the other.

We use the following criterion: $\Delta x \leq \frac{1}{5}\left(\frac{v_{min}}{f}\right)$ (Linzer et al., 2021). Where Δx is the grid size, v_{min} is the minimum shear velocity and f is the frequency of the source. Given that the slowest shear velocity (Quartzite, v_{min} = 3200 m/s), period is 0.015 s ($f = \frac{1}{0.015}$ = 66 Hz), which just meets the criterion since $\Delta x = 10 \sim \frac{1}{5}\left(\frac{3200}{66}\right)$.

2D waveform processing

3-component recievers are placed according to different configurations (described in the case studies) which can be viewed on the mXrap version 6 platform (Harris and Wesseloo, 2024). The z-component (vertical) of the waveforms was recorded and stored on each reciever (history). Recording channels on each receiver were assigned individual travel-times and consequently converted to seismic traces using ObsPy (a Python framework dedicated to processing seismological data). The sesimic traces were finally converted to SEG-Y format which was used to produce one-way traveltime shotgathers.

The model is constrained in a bounding box with dimensions 2000 m x 2200 m x 3950 m and has a grid size of 10 m. One of the main aims of the survey is to determine whether one can detect and characterise the seismic wavefield reflected by the BLR, VCR, and mine tunnels from the receivers on surface. In order to do this, a simulated source is placed in the tunnel at a depth of 3800 m and the 3-component receivers are 'buried' at ~10 m below surface (next to the tailing storage facilities). The source and receiver parameters can be found in Table 1. The result of this model set-up is a 3D cube, which is divided into three lithologies, i.e., dolostone, Ventersdorp andesitic basalts, and quartzites as illustrated in Figure 5. Each lithology is assigned its own seismic velocities and densities.

Following, is an investigation of two case studies where we explore two experimental configurations. The first case study (Figure 6) explores the conventional seismic reflection survey set-up whereby the source and receivers are located on surface and the wavefield is propagated from the surface through the interfaces below surface. In the second case study (Figure 8), the source is placed at a depth of 3800 m below surface and the receivers on surface, and the wavefield is propagated from underground to surface. The parameters used in the case studies are listed in Table 1 and 2.

Case study 1: Source and receivers located on surface

The conventional set-up shows well defined BLR and VCR interfaces (Figure 6a). The source produced clear P- and S-wave first arrivals and the subsequent waves can be seen interfering with each other and producing multiple secondary waves as the

Table 1

Physical properties and numerical modelling parameters used in the study

Physical properties			
Material	**P-wave velocity (m/s)**	**S-wave velocity (m/s)**	**Density (g/m³)**
Country rock (quartzite)	5800	3200	2.67
Pseudo-air (in tunnel)[1]	340	1	1
Dolostone	6700	4200	2.9
Ventersdorp basaltic andesites	6200	3500	3
Quartzite	5800	3200	2.67
Source parameters			
Source type	**Waveform**	**Amplitude (Pa)**	**Period (s)**
Dilatational	Smooth step	10^6	0.015
Receiver parameters			
Frequency (Hz)	**Spacing (m)**		
0–700	10		

[1]WAVE3D is an elastic code and cannot model air (gas), hence we use pseudo-air which is a very soft material having low velocity and low density

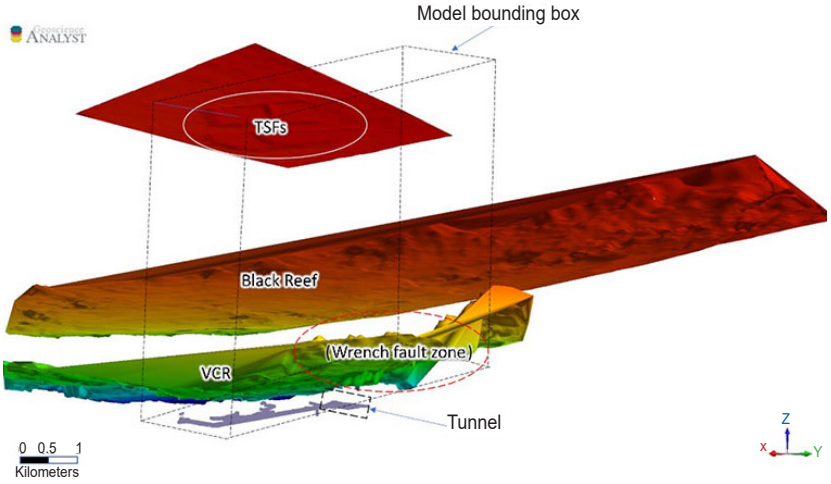

Figure 4—A 3D model illustrating the relative locations of the tailing storage facilities (TSF), Black Reef, Ventersdorp Contact Reef (VCR), and the mine tunnels

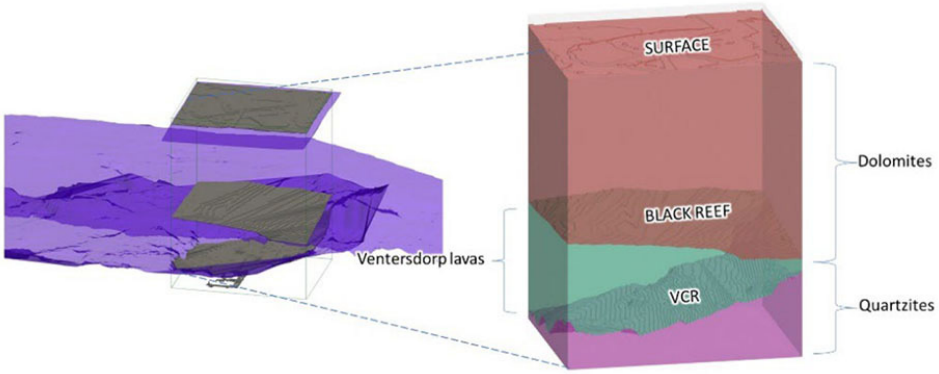

Figure 5—A 3D cube showing the simplified model, which was extracted from a larger, complex model

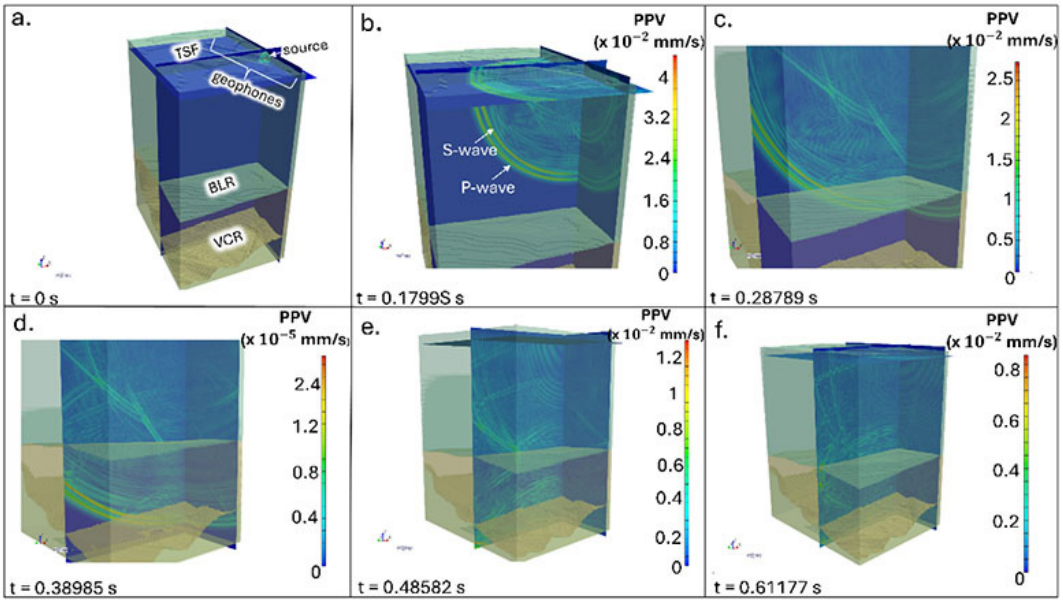

Figure 6—A snapshot sequence showing the propagation and peak particle velocity (PPV) of the wavefield at different times. (a – f) wavefield snapshot at t = 0 s to t = 0.61177 s, showing the P- and S-wave as well as possible reflections from the dolostone – andesitic basalt, andesitic basalt – quartzite interfaces

wavefield propagates through the dolostone (Figure 6b). When the wavefront interferes with the dolostone – andesitic basalt (BLR) interface (Figure 6c), it is mostly refracted but one can also observe few reflections. The dilatational source (amplitude of 10^6Pa) used in the model resulted in consistent ground motion throughout the volume of the model. This is indicated by the peak particle velocity (PPV) which varies between 0.0015 – 0.002 mm/s after ~0.29 s of the source's initiation. In Figure 6d, the wavefield interacts with the

Table 2

Calculated parameters used in the study

Material	Young's modulus (GPa)	Shear modulus (GPa)	Bulk modulus (GPa)	Poisson's ratio (ν)	P-wave modulus[2] (GPa)
Country rock (quartzite)	70	27	53	0.28	90
Pseudo-air (tunnel)	0.12	0.11	0.12	0.499	0.12
Dolostone	120	130	61	0.176	130
Quartzite	70	27	53	0.28	90
Ventersdorp andesitic basalt	93	115	66	0.27	115

[2]P-wave modulus is defined as the ratio of axial stress to axial strain in uniaxial strain state, which is equivalent to stating that $M = \rho V_p^2$, where V_p is the velocity of the P-wave and ρ is the density of the medium in which the wave is propagating through

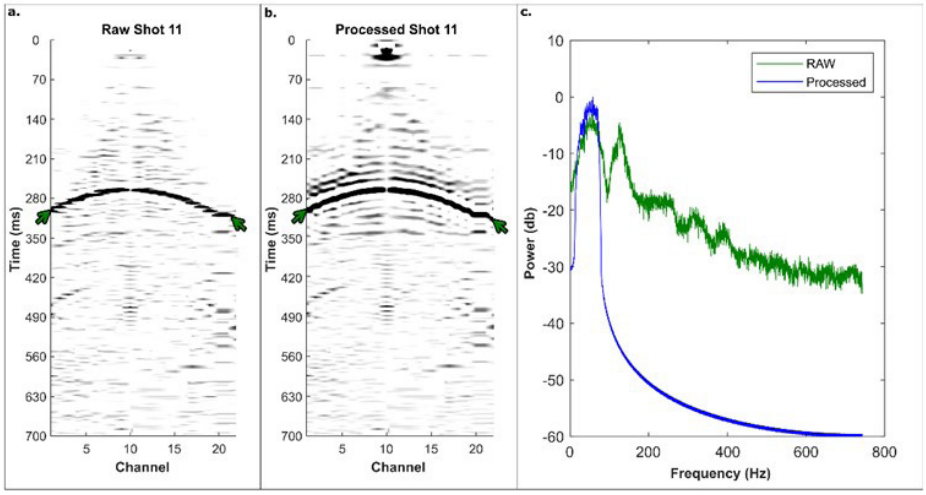

Figure 7—(a) A raw shot gather (shot 11) showing the different arrivals times from the simulation in 700 ms timeframe. (b) Processed shot gather showing the different arrivals times from the simulation in 700 ms timeframe. The green arrows showing possible reflections. (c) Frequency-power spectrum showing the effect of ACG and bandpass filtering

andesitic basalt - quartzite (VCR) interface and we observe much stronger P-wave reflections. After passing through the interface, we observe a significant decrease in ground motion due to the seismic wave's propagation and this is indicated by PPV decreasing almost a thousand times from the previous snapshot (i.e. Figure 6c). Near the vicinity of the tunnel (Figure 6e and 6f), the wavefield continues to interact with both of the interfaces and the ground motion velocity averages ~0.06 mm/s in the period 0.49 – 0.61 s after the initiation of the source.

The shotgather (central shot 11) from case study 1 show multiple travel times . An amplitude gain control (AGC) filter is applied to enhance the faint arrivals from the raw shotgather (Figure 7a and 7b). Multiple first arrivals between 220 ms and 280 ms are observed, which are intepreted to represent P-and S-waves first arrivals. These arrivals are followed by P-wave and S-wave reflection events between 280 ms and 350 ms. The strong P-wave reflection observed between 280 ms and 350 ms, represented by the green arrow in Figure 7b, is interpreted to originate from the VCR horizon. One can also observe consistent artificial arrivals, which are a result of boundary conditions of the computational set-up. A bandpass filter [0 10 140 160] Hz is applied in Figure 7c.

Case study 2: Source inside the tunnel and receivers on surface

This unique set-up illustrates how the seismic wavefield behaves as it travels from its source located in a tunnel, through the BLR and VCR interfaces and as it reaches the receivers on surface. From its inception, the wavefield shows well defined P- and S-wave arrivals (Figure 8a). One observes reflections coming off the quartzite – andesitic basalt (VCR) interface. These reflections result in ground motion with PPVs between 0.12 mm/s and 0.06 mm/s. Along the outer edges of the tunnel, we observe significantly higher PPVs (<0.12 mm/s). This range of observed PPV values is influenced, amongst other factors, by the amplitude (10^6 Pa) of the dilatational source. In Figure 8b, we observe that the wavefield undergoes much less interference as it passes through the lava-dolostone (BLR) boundary. The direction of the wavefront and the PPV remain fairly constant. One can still observe the multiple reflections coming off the geological layers, including the VCR and Black Reef surfaces , but at lower PPVs (> 0.06 mm/s).

Figure 9a shows a time delay (~ 400 ms) of P-wave first arrivals due to the distance (~ 3000 m) between the underground source and the receivers on surface. We apply an amplitude gain control (AGC) filter to enhance the faint arrivals from the raw shotgather (Figure 9a and 9b). A bandpass filter [0 10 140 160] Hz is applied in Figure 9c. A series of high amplitude reflection events can also be seen between 350 ms and 700 ms (indicated by green arrows in Figure in 9b) after bandpass filtering. At this stage it is not clear what these reflections represent, however these could represent the P-wave and S-wave reflections from the Black Reef and VCR horizons.

Conclusion

The use of finite difference modelling to simulate surface and

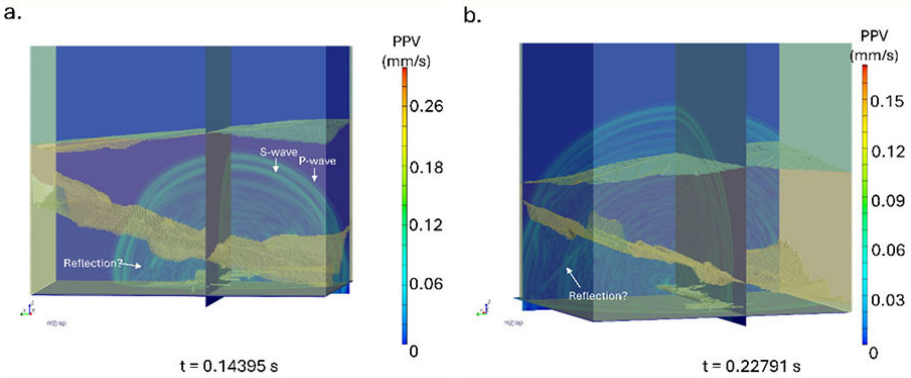

Figure 8—A snapshot sequence showing the propagation and peak particle velocity (PPV) of the wavefield at different times. (a) Wavefield snapshot at t = 0.14395 s, showing the P- and S-wave as well as possible reflections from the quartzite - andesitic basalt interface. (b) wavefield snapshot at t = 0.22791 s

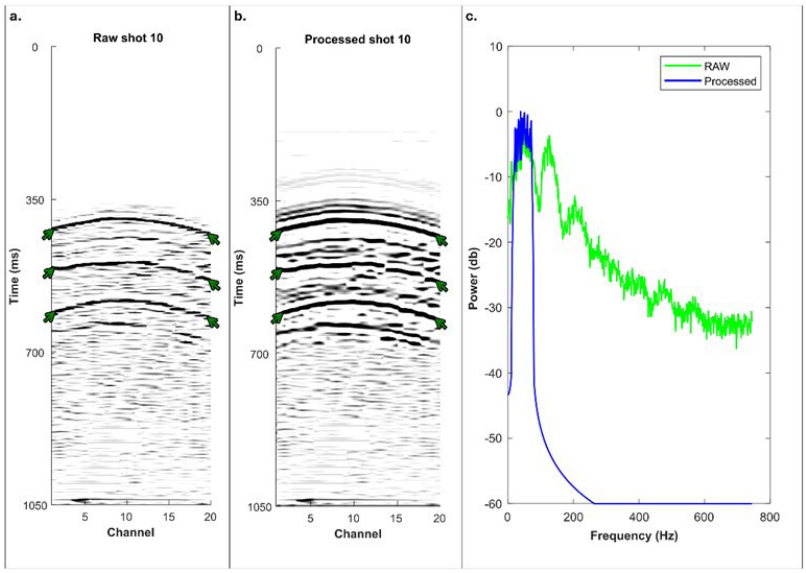

Figure 9—(a) A raw shot gather (shot 10) showing the different arrival times from the simulation in 1050 ms timeframe. The green arrows showing possible reflections from the Ventersdorp Contact Reef and Black Reef. (b) Processed shot gather showing the different arrivals times from the simulation in 1050 ms timeframe. (c) Frequency-power spectrum showing the effect of ACG and bandpass filtering

in-mine reflection seismic surveys revealed useful information about the subsurface geology at South Deep Gold Mine. When we compare both case studies, we note the following:

- The configuration of sensors and sources used in the simulations reveal that the seismic wavefield can be recorded from depths close to 4 km below surface. Moreso, both case studies show that the wavefield produced by our source can be used to successfully image the Black Reef (BLR) and Ventersdorp Contact Reef (VCR).
- In both case studies, the secondary wavelets undergo mutiple mode conversions even before interacting with the BLR and VCR. These conversions occur much more rapidly when the wavefield interacts with the outer edges of the tunnel.
- P- and S-waves tend to interact with the tunnel walls, potentially reflecting, refracting, or converting into other wave modes. When surface waves propagate on the tunnel edge, although they are much slower than the body waves, they carry a significant amount of energy along the surface.
- We also note that the wavefield's behaviour in our simulation is influenced by several factors which include material properties (e.g. reflection and transmission coeffecients due to contrast between the tunnel and the country rock surrounding it) and frequency content i.e lower frequencies interact with the bulk structure of the tunnel and higher frequencies are sensitives to small-scale features in the geometry.
- In the first case, a clear P-wave arrival is recorded at ~290 ms. The velocity of the dolostone layer is 6700 m/s, consequently this corresponds to a depth of 1943 m below surface.

These results were used to constrain the design and acquisition of the seismic surveys conducted inside the mine tunnels at South Deep Gold Mine. For example, when conducting an actual reflection seismic survey, we can anticipate that the edges of the underground tunnel will be the main cause of the wavefield's PPV changes followed by the BLR and VCR interfaces. As such, this would influence the choice of source and receiver parameters utilised in the survey as well as the configuration of sensors used in both case studies. In doing so, one can optimise the design parameters for future surface and in-mine seismic surveys for deep orebody imaging, mine planning, and development .

Acknowledgement

This research is funded by the FUTURE project of ERA-NET Cofund on Raw Materials (ERA-MIN3), Advanced Orebody Knowledge (AOK), and DSI-NRF Centre of Excellence (COE)

for Integrated Mineral and Energy Resource Analysis (CIMERA). Computational resources were provided by SRK Consulting (South Africa) (Pty) Ltd for WAVE3D. Further acknowledgement goes to the Australian Centre for Geomechanics (ACG) and Mira Geoscience for providing the software mXrap and Geoscience ANALYST, respectively.

We thank South Deep Gold Mine for providing us with mine data as well as granting us the permission to publish this research.

References

De Kock, W.P. 1964. The geology and economic significance of the West Wits Line. Haughton, S.H. (Ed.). The Geology of Some Ore Deposits of Southern Africa, 1. *Geological Society of South Africa*, Johannesburg, pp. 323–386.

Durrheim, R.J., Nicolaysen, L.O., Corner, B. 1991. A deep seismic reflection profile across the Archean-Proterozoic Witwatersrand Basin, South Africa. *Continental lithosphere: Deep seismic reflections*, vol. 22, pp. 213–224.

Gibson, M.A.S., Jolley, S.J., Barnicoat, A.C. 2000. Interpretation of the Western Ultra Deep Levels 3D seismic survey. *The Leading Edge,* vol. 19, pp. 730–735.

Gibson, M.A.S. 2004. Goldfields KEA 3D Seismic Project: Final Report. Unpublished report to Gold Fields Mining, pp. 52.

Gibson, M.A.S. 2005. Interpretation of the 2003 South Deep 3D Seismic Survey. Unpublished report to Gold Fields Mining, pp. 62.

Harris P.C, Wesseloo J. mXrap software., (2015). Perth, Western Australia, *Australian Centre for Geomechanics*, The University of Western Australia, version 5. http://mxrap.com/

Hildyard, M.W., Daehnke, A. Cundall, P.A. 1995. WAVE: A computer program for investigating elastodynamic issues in mining. *Proceedings of the 35th US Symposium on Rock Mechanics*. Balkema, Rotterdam. pp. 519–524.

Jolley, S.J., Freeman, S.R., Barnicoat, A.C., Phillips, G.M., Knipe, R.J., Pather, A . 2004. Structural controls on Witwatersrand gold mineraliation. *Journal of Structural Geology*, vol. 26, nos. 6–7, pp. 1067–1086.

Kositcin, N., Krapež, B. 2004. Relationship between detrital zircon age-spectra and the tectonic evolution of the Late Archaean Witwatersrand Basin, South Africa. *Precambrian Research*, vol. 129, nos. 1–2, pp. 141–168.

Krapež, B. 1985. The Ventersdorp Contact Placer: a gold/pyrite placer of stream and debris-flow origin from the Archaean Witwatersrand Basin of South Africa. *J. Sediment.*, vol. 32. pp. 223–234.

Linzer, L., Hildyard, M., Wesseloo, J. 2021. Complexities of underground mining seismic sources. *Philosophical Transactions of the Royal Society A: Mathematical, Physical and Engineering Sciences*. 379. 20200134. 10.1098/rsta.2020.0134.

Manzi, M.S., Gibson, M.A., Hein, K.A., King, N., Durrheim, R.J. 2012. Application of 3D seismic techniques to evaluate ore resources in the West Wits Line goldfield and portions of the West Rand goldfield, South Africa. *Geophysics*, vol. 77, no. 5, pp. 163–171.

Manzi, M.S.D., Hein, K.A.A., Durrheim, R., King, N. 2013. Seismic attribute analysis to enhance detection of thin gold-bearing reefs: South Deep gold mine, Witwatersrand basin, South Africa. *Journal of Applied Geophysics*, vol. 98, pp. 212–228.

McCarthy, T.S. 2006. The Witwatersrand Supergroup. Johnson, M.R., Anhaeusser, C.R., Thomas, R.J. (Eds.), The Geology of South Africa. Geological Society of South Africa, Johannesburg. Council for Geosciences, Pretoria, pp. 155–186.

Myers, R.E., McCarthy, T.S., Stanistreet, I.G. 1989. A tectono-sedimentary reconstruction of the development of the Witwatersrand Basin, with particular emphasis on the Central Rand Group. *Economic Geology Research Unit Information Circular*, 216, pp. 497–540.

Nwaila G.T., Bourdeau, J.E., Jinnah, Z., Frimmel H.E, Bybee G.M, Zhang SE, Manzi M.S.D, Minter W.E.L., Mashaba D. 2021. The Significance of Erosion Channels on Gold Metallogeny in the Witwatersrand Basin (South Africa): Evidence from the Carbon Leader Reef in the Carletonville Gold Field. *Economic Geology*, 116, pp. 265–284.

Van der Westhuizen, W.A., De Bruiyn, H., Meintjes, P.G. 1991. The Ventersdorp Supergroup: an overview. *Journal of African Earth Sciences*, vol. 13, pp. 83–105.

Vos, R.G. 1975. An alluvial plain and lacustrine model for the Precambrian Witwatersrand deposits of South Africa. *Journal of Sedimentary Petrology* vol. 45, pp. 480–493. ◆